AIAA JOURNAL
Vol. 47, No. 12, December 2009

Analysis and Simulation of Optimal Vibration Attenuation for Underactuated Mechanical Systems

S. Woods* and W. Szyszkowski†
University of Saskatchewan, Saskatoon, Saskatchewan S7N 5A9, Canada

DOI: 10.2514/1.40158

This paper deals with active optimal vibration attenuation of elastic structures modeled by finite elements. The system's equations are linear with potentially large numbers of degrees of freedom, whereas the minimized performance index is quadratic. The problem is formulated in modal space so that the dimension of the problem can be limited to controlling significant modes only. Their number is considered greater than the number of independent discrete actuators, making the system underactuated. The constraints resulting from underactuation are represented by the matrix of constraints that couples the modal controls. This matrix, which plays an important role in predicting the systems controllability, is obtained by adding a set of dummy actuators. The modal variables are in turn coupled via second-order nonholonomic constraints, which are satisfied with the help of time-dependent Lagrange multipliers. The optimality equations for the problem are derived in a compact form and solved by applying symbolic differential operators. The procedure, which applies standard finite element and mathematical software, renders the optimal actuation forces and the response of all controlled modes, or any selected degrees of freedom, for the entire control process. Two simulation examples are presented to illustrate the approach's details and the use of controllability indicators derived from the matrix of constraints.

Nomenclature

$A[a_{ij}]$	=	normalized matrix of constraints
A_a, A_r	=	partition of matrix A
a	=	coefficient weighting strain energy in the performance index
B	=	actuators' placement matrix
$\hat{B}$	=	matrix relating the actuators to modal controls for fully actuated systems
$\bar{B}$	=	transfer matrix (from modal controls to actuators) for fully actuated systems
$\bar{B}_a$	=	pseudotransfer matrix for underactuated systems
$\hat{B}'$	=	matrix relating the actuators to modal controls for the systems with dummy actuators
b	=	coefficient weighting kinetic energy in the performance index
C	=	Rayleigh damping matrix
c	=	coefficient weighting power of actuators in the performance index
c^i_{kj}	=	integration constants
D, $\hat{D}_{ij}$, $\tilde{D}_{ij}$	=	differential operators
d^i_k	=	displacement of node i in direction k
E, $\tilde{E}$, E_i	=	differential operators
F	=	vector of nodal forces
F_a	=	vector of forces in actuators
F_d	=	vector of forces in dummy actuators
G	=	gain matrix
H	=	augmented Hamiltonian
J	=	performance index
K	=	stiffness matrix
M	=	mass matrix
n	=	number of degrees of freedom
n_a	=	number of independent actuators
n_m	=	number of controlled modes
n_r	=	number of redundant modes (or constraints)
P_d, P_v	=	vector of costates
$\hat{Q}_d$, $\hat{Q}_v$, $\hat{R}$	=	diagonal matrices in performance index
t^{eff}_k	=	effective settling time for k frequency
U	=	vector of modal controls
U_a, U_r	=	independent and redundant modal controls
X	=	vector of degrees of freedom
α_k, β_k	=	roots of characteristic equation
η	=	vector of modal variables
η_a, η_r	=	independent and redundant modal variables
λ, κ	=	rate and effort controllability indicators
ξ_i	=	damping ratio for frequency i
ϕ_i	=	modal shapes
Ω	=	diagonal matrix of ordered frequencies
ω_i	=	frequency of mode i

Received 30 July 2008; revision received 29 January 2009; accepted for publication 10 September 2009.

*Graduate Student, Department of Mechanical Engineering (Corresponding Author).

†Professor, Department of Mechanical Engineering, Walerian.Szyszkowski@usask.ca.

I. Introduction

MECHANICAL systems with fewer actuators than the number of the degrees of freedom (DOF) are referred to as underactuated [1–4]. Thus, any vibrating structural system with continuous elastic members (and, theoretically, infinite DOF) controlled by discrete actuators is underactuated. When such systems are modeled using the finite element (FE) method, the number of DOF, though finite, is usually very large in comparison with the number of actuators. Many structural systems can be analyzed by the modal superposition method, which provides sufficient accuracy by considering a relatively small number of modes [5] to be referred to as significant. The problem is still underactuated if the number of significant modes (output size), representing the system's generalized DOF, is greater than the number of actuators (input size).

The DOF of an underactuated system are coupled by nonintegrable (nonholonomic) constraints arising from the equations of motion, which impose some restrictions on its possible movements. Also, underactuation complicates the inverse dynamics needed to determine actuation forces because only trajectories that satisfy the nonintegrable constraints are physically realizable. Generally, control of underactuated systems is associated with the so-called nonminimum phase features, leading to unbounded behaviors [6,7]. This is mostly due to the inverse dynamics becoming unstable (i.e., generating unstable zeros) when attempting to follow desired

trajectories that do not satisfy the constraints resulting from underactuation [8].

To avoid the unstable inverse dynamics when analyzing underactuated systems, the noncausal methods were proposed and applied mainly to flexible manipulators in [9–11]. However, these methods were somewhat "nonphysical" and demonstrated questionable convergence (in fact, the presence and consequences of the nonholonomic constraints appear to have been overlooked in these papers).

Some underactuated problems with passive joints, related mostly to tracking problems, have been analyzed by first removing the redundant DOF and then solving the reduced fully actuated problems, with a number of actuators controlling the same number of independent DOF [12–18]. For fully actuated problems, the independent modal space control (IMSC) method may be applied, with its main advantage being that each modal variable is directly related to a corresponding independent modal control [19]. In these cases, the solution involves the "input space" because the problem size was reduced to the input size. This approach is limited to cases in which the elimination of redundant variables is possible (exactly or approximately), and it typically requires extensive analytical effort.

The method of active optimal vibration attenuation of elastic structures presented in this paper obtains solutions in the "output space" with the problem size equal to the number of controlled modes. Instead of attempting to *eliminate* redundant modes (or redundant DOF) to make their total number equal to the number of actuators, "dummy" actuators are *added* to make the total number of actuators equal to the number of significant modes. The dummy actuators are subsequently eliminated by applying the constraints, which are nonholonomic in terms of the modal variables, but algebraic when imposed on the modal controls. A matrix of constraints is defined for a particular configuration of actuators, with its terms containing information on the system's controllability and attenuation characteristics. The constraints are satisfied with the use of time-dependent Lagrange multipliers. Optimality equations are derived as a set of coupled differential equations involving all the modal variables and Lagrange multipliers. These equations are then solved by applying symbolic operators to provide the optimal input (actuation forces) and output (system response). Such an approach can be referred to as the constrained modal space optimal control (CMSOC) to distinguish it from the IMSC method. Finally, the solution can be verified by directly applying the actuation forces to the FE model of the system (which may contain a much larger number of modes than that considered in the control).

Because the constraints due to underactuation are always satisfied, the problem of unstable inverse dynamics is formally eliminated. The effectiveness of particular actuator locations on controlling a particular number of vibration modes, or the controllability of the system, can be evaluated before simulating the control process. In particular, in the case of poor controllability, the CMSOC can predict whether the system will respond with excessively high actuation forces or very slow rates of attenuation in certain modes.

The basic steps of our approach are demonstrated on a 2-DOF problem analyzed in example I in Sec. V. Example II, in Sec. VI, tackles a 120-DOF problem that focuses more on the system's controllability, which can be evaluated at the early stage of the simulation by using certain numerical indicators derived from the matrix of constraints.

II. Problem Formulation

The optimal active vibration control of discrete or continuous elastic mechanical systems, represented by FE models with sufficient DOF, is analyzed. It is assumed that the equations of motion for the system take the following form:

$$M\ddot{X} + C\dot{X} + KX = BF_a(t) = F \tag{1}$$

where M,C, and K are the constant mass, natural damping, and stiffness matrices, respectively. The actuation force vector with n_a independent components is denoted by $F_a(t)$. The system's DOF are represented by vector X with n components (typically $n_a \ll n$). Matrix B $(n \times n_a)$ assigns the actuation forces to the DOF, and F is the corresponding nodal force vector. Formally, n_a actuation forces are to control n DOF describing the system's motion, and so there must be $n_r = n - n_a$ additional constraints to be satisfied by all DOF.

The objective is to apply actuation forces as effectively as possible to eliminate vibration energy. Such a task can be formulated in terms of minimizing the performance index defined as follows:

$$J = \frac{1}{2}\int_o^\infty (aX^TKX + b\dot{X}^TM\dot{X} + cF^TK^{-1}F)\,\mathrm{d}t \to \min \tag{2}$$

Weighting coefficients a, b, and c are assigned to the system's elastic energy (potential), kinetic energy, and the work (or power) of the actuation forces, respectively. Such a quadratic performance index is routinely used in vibration control of flexible structures [20].

Equations (1) and (2) formally represent the linear quadratic regulator problem with $2n$ states and n_a controls. Note that one would normally have to solve nonlinear algebraic Riccati equations for the unknown terms of a symmetric matrix of size $2n$, or $2n^2 + n$ unknowns altogether, meaning that the problem presented in example II would have 28,920 unknowns, which is prohibitively large for any numerical handling [20]. Our approach does not use Riccati's equations at all.

The problem defined by Eqs. (1) and (2) can be mapped into the modal space, where modal frequencies ω_i and corresponding modal shapes ϕ_i are the solutions of the eigenvalues problem $(K - \omega_i^2 M)\phi_i = 0$. The modal shapes matrix $\phi = [\phi_1, \ldots, \phi_n]$ satisfies the following orthogonality conditions:

$$\phi^TM\phi = I \tag{3a}$$

$$\phi^TK\phi = \Omega \tag{3b}$$

where I is a unit matrix, and Ω is a diagonal matrix of ordered frequencies with the terms $\Omega_{ii} = \omega_i^2$.

Vectors X and F in Eqs. (1) and (2) are replaced by vectors of modal variables η and modal forces U, respectively, through the following transformations:

$$X = \phi\eta \tag{4a}$$

$$U = \phi^TF \tag{4b}$$

With C assumed as a Rayleigh matrix, the equations of motion (1) become uncoupled in modal space, taking the following form:

$$I\ddot{\eta} + \Delta\dot{\eta} + \Omega\eta = U \quad \text{or} \quad \ddot{\eta}_i + 2\zeta_i\omega_i\dot{\eta}_i + \omega_i^2\eta_i = u_i \qquad i = 1, 2, \ldots \tag{5}$$

where $\Delta_{ii} = 2\zeta_i\omega_i$ and $\zeta_i = \phi_i^TC\phi_i/(2\omega_i)$ are passive modal damping ratios. The numbers of modal variables and modal controls in Eq. (5) are identical, so that the direct and inverse mapping between the controls U and variables η is always possible in the modal space.

Substituting Eqs. (4a) and (4b) into Eq. (2) and using Eqs. (3a) and (3b), the performance index is transformed into

$$J = \frac{1}{2}\int_o^\infty (\eta^T\hat{Q}_d\eta + \dot{\eta}^T\hat{Q}_v\dot{\eta} + U^T\hat{R}U)\,\mathrm{d}t \tag{6}$$

The new weighting matrices in the transformed performance index (6) are diagonal and equal to $\hat{Q}_d = a\Omega$, $\hat{Q}_v = bI$, and $\hat{R} = c\Omega^{-1}$.

Equations of motion (5) and performance index (6) in the modal space are formally equivalent to Eqs. (1) and (2), respectively (the latter define the problem in terms of DOF). The benefit of using modal space in computational dynamics lies in the possibility of obtaining acceptable solutions for systems with a large number of DOF (or continuous systems) by considering only n_m significant modes, where $n_m \ll n$ (see [5] for physical and numerical justifications). The number of significant modes that might be

required in modeling a structure is generally problem related and depends mainly on its physical characteristics, the spatial distribution, and the frequency content of the loading.

The first n_a significant modal variables, which might be viewed as controlled directly by n_a independent actuators, are referred to as independent, whereas the remaining $n_r = n_m - n_a$ modal variables, as controlled indirectly, are referred to as redundant. Redundant variables are related to the independent ones by n_r constraints, which are discussed in detail later in this section.

Because only the first n_m vibration modes are considered significant, the reduced modal shape matrix $\tilde{\phi} = [\phi_1, \ldots, \phi_{n_m}]$ of size $n \times n_m$ is required in the transformations (4a) and (4b). It is assumed that the modal shape matrix $\tilde{\phi}$ of sufficient size and accuracy is available from the FE software (ANSYS was used for this purpose).

All n_m components of U driving the significant modes, for a given vector F_a, are obtained from

$$U = \tilde{\phi}^T B F_a = \hat{B} F_a \tag{7}$$

also divided into a vector of *independent* modal controls $U_a = [\,u_1 \;\; \cdots \;\; u_{n_a}\,]^T$ and a vector of *redundant* modal controls $U_r = [\,u_{n_a+1} \;\; \cdots \;\; u_{n_m}\,]^T$. Both controls are determined, but only U_a will be required for determining the actuation forces.

Because $F_d = 0$, the rows in the lower partition of form (8) define the set of n_r constraints, linear in terms of U, which can be written in the form of homogeneous equations:

$$h(u_1, \ldots, u_m) = A_a U_a + A_r U_r = AU = 0 \tag{9}$$

Matrix $A = [\,A_a \quad A_r\,]$ of size $n_r \times n_m$, to be referred to as the matrix of constraints, may be fully populated with $n_c n_m$ nonzero coefficients a_{ij}. However, because Eq. (9) is homogeneous, these coefficients can be normalized such that $a_{ii} = 1$ and $a_{k,i} = 0$ for $k > i$ (left bottom corner) and $a_{k,n_a+1+k} = 0$ for $1 \le k \le n_r - 1$ (right upper corner). This gives the following form:

$$A = \left[\begin{array}{ccccccccccc} 1 & a_{12} & a_{13} & \ldots & a_{1,n_r} & \ldots & a_{1,n_a} & a_{1,n_{a+1}} & & & \\ & 1 & a_{23} & \ldots & a_{2,n_r} & \ldots & a_{2,n_a} & a_{2,n_{a+1}} & a_{2,n_a+2} & & \\ & & 1 & \ldots & \ldots & \ldots & \ldots & \ldots & \ldots & & \\ & & & \ldots & \ldots & \ldots & \ldots & \ldots & \ldots & \ldots & \\ & & & & 1 & \ldots & a_{n_r,n_a} & a_{n_r,n_a+1} & a_{n_r,n_a+2} & \ldots & a_{n_r,n_m} \end{array}\right] \tag{10}$$

(A_a: columns 1 through n_a; A_r: columns n_a+1 through n_m)

The dimensions of matrix $\hat{B} = \tilde{\phi}^T B$ are $n_m \times n_a$. Operation (7) is always possible in the *direct* dynamics, but in control analysis vector F_a is to be determined (the *inverse* dynamics); therefore, Eq. (7) is used in reverse order. Then this vector is to generate the modal control vector U that in turn drives modal variable vector η and finally the desired vector X of system DOF.

If the number of actuators n_a is equal to the number of significant modes n_m (fully actuated) the inversion of Eq. (7) requires a nonsingular matrix $\hat{B}$ of dimensions $n_a \times n_a$ such that the vector of actuation forces can be obtained from $F_a = \hat{B}^{-1} U$. Therefore, matrix $\bar{B} = \hat{B}^{-1}$, transferring the modal controls into actuator forces, can be related to controllability because it directly implies whether or not the actuators are capable of controlling all the modes that define the system dynamics [recall that the modal controls can always be mapped into the modal variables by applying Eq. (5)].

This reasoning can be extended to the underactuated system for which $n_a < n_m$. The aforementioned $n_r = n_m - n_a$ additional constraints for the system can be explicitly determined by sequentially *eliminating* the n_a components of vector F_a from Eq. (7) to obtain the extra conditions to be satisfied by all n_m components of vector U. Alternatively, these conditions can be obtained by *adding* n_r dummy (zero-value) actuators F_d to the system's n_a real actuators F_a. The only restriction on dummy actuator placement is that the corresponding square matrix $\hat{B}'$ (of size $n_m \times n_m$) is nonsingular. With dummy actuators included, the new $(\hat{B}')^{-1}$ can be calculated and partitioned so that the inverse operation of Eq. (7) takes the following form:

$$\begin{bmatrix} F_a \\ F_d \end{bmatrix} = (\hat{B}')^{-1} U = \begin{bmatrix} \tilde{B}_a & \tilde{B}_r \\ A_a & A_r \end{bmatrix} \begin{bmatrix} U_a \\ U_r \end{bmatrix} = \begin{bmatrix} F_a \\ 0 \end{bmatrix} \tag{8}$$

The dimensions of square matrices $\tilde{B}_a$ and A_r are $n_a \times n_a$ and $n_r \times n_r$, respectively. To be consistent with the division of the modal variables into independent and redundant, vector $U = [\,U_a^T \quad U_r^T\,]^T$ is

This normalized form of A is independent of the selection of dummy actuators because their role is only to facilitate the process of eliminating F_a from Eq. (7), as already mentioned. Hence, matrix A represents the system's configuration of real actuators and will be used for evaluating its controllability.

Real actuation force vector F_a may be generated from the full modal control vector $U = [\,U_a^T \quad U_r^T\,]^T$ through the top partition of form (8) (i.e., $F_a = \tilde{B}_a U_a + \tilde{B}_r U_r$). However, using the constraint (9) to eliminate U_r, the actuation forces can be obtained solely in terms of the components of independent modal control vector U_a in the following form:

$$F_a = \bar{B}_a U_a \quad \text{where } \bar{B}_a = \tilde{B}_a - \tilde{B}_r A_r^{-1} A_a \tag{11}$$

The dimensions of square matrix $\bar{B}_a$ are $n_a \times n_a$. This matrix, similar to matrix A, is independent of the selection of dummy actuators. If a problem is fully actuated ($n_m = n_a$), then $\bar{B}_a = \bar{B}$. Equation (11) requires the nonsingularity of matrix A_r; otherwise. Eq. (9) cannot be used to determine the redundant controls in terms of the independent controls. Matrix $\bar{B}_a$, referred to as the pseudotransfer matrix because it has a similar physical interpretation as matrix $\bar{B}$ for fully actuated systems [see Eq. (7)], must also be nonsingular. More details about obtaining matrices A and $\bar{B}_a$ are given in Sec. V, in which example I is presented.

Matrices A_r and $\bar{B}_a$ can be considered indicators of controllability. Thus, the following two numerical measures, λ and κ, referred to as the rate and effort parameters, respectively, are adopted to reflect control performance (or the effectiveness of certain actuators' locations):

$$\lambda = |\det A_r| \tag{12a}$$

$$\kappa = |\det \bar{B}_a| \tag{12b}$$

The first parameter reflects the rate of attenuating the system's disturbances, whereas the second is related to the actuation forces

required in the process. Such "physical" interpretations of these parameters will be illustrated in Sec. VI, in which example II is presented.

The controllability parameters can be used only to compare different configurations of actuators for a particular mechanical system. Note that matrix A_r in Eq. (12a), which represents the last n_r columns of the normalized matrix A in Eq. (10), is always triangular so that $\det A_r = a_{1,n_a+1} \times a_{2,n_a+2} \times \cdots \times a_{n_r,n_m}$. Ideally the best rate of attenuation of all modes is achieved if all nonzero elements of matrix A_r have a value of unity, and so $\lambda = |\det A_r| = 1$. This is because for such locations of actuators the redundant modal controls will have similar magnitudes as the independent modal controls. Consequently, in the CMSOC, the redundant modal variables will be attenuated at a similar rate as the independent modal variables, which in turn are attenuated according to the IMSC scheme.

Actuator locations with smaller values of effort parameter κ will generally have smaller maximum force requirements. This is because the independent modal controls are determined first, irrespective of actuator positioning, and next mapped into the actuation forces.

Formally, the equations of dynamics (5), with constraints (9), and performance index (6) completely define the optimization problem with n_a independent actuators (the input size) in the n_m-dimensional modal space (the output size). Such problems can be solved by applying the optimality conditions, which are derived next.

III. Optimality Equations

The optimality conditions for the problem defined by Eqs. (5) and (6) and constraint (9) will be derived from Pontryagin's principle. Treating η and $\dot{\eta}$ as vectors of independent state variables, the *augmented* Hamiltonian can be written as follows:

$$H = -\tfrac{1}{2}(\eta^T \hat{Q}_d \eta + \dot{\eta}^T \hat{Q}_v \dot{\eta} + U^T \hat{R} U + \Gamma) + P_d^T \dot{\eta} + P_v^T(-\Delta\dot{\eta} - \Omega\eta + U) + v^T A U \tag{13}$$

Vectors P_d and P_v are standard costates related to the states (η and $\dot{\eta}$, respectively). Vector $v^T = [\, v_1 \quad \cdots \quad v_{n_r} \,]$ represents the set of time-dependent Lagrange multipliers introduced to enforce the constraints (9). Applying the Pontryagin formalism, the costate equations for the problem are obtained in the following form:

$$\dot{P}_d = -\partial H/\partial\eta = \hat{Q}_d \eta + \Omega P_v \tag{14a}$$

$$\dot{P}_v = -\partial H/\partial\dot{\eta} = \hat{Q}_v \dot{\eta} - P_d + \Delta P_v \tag{14b}$$

The Hamiltonian is stationary with respect to modal control if

$$\partial H/\partial U = -\hat{R}U + P_v + A^T v = 0 \tag{15}$$

Substituting Eq. (5) into Eq. (15) renders

$$P_v = \hat{R}(I\ddot{\eta} + \Delta\dot{\eta} + \Omega\eta) - A^T v \tag{16}$$

Substituting Eq. (16) into Eq. (14b) yields

$$P_d = \hat{Q}_v \dot{\eta} - \hat{R}(I\dddot{\eta} + \Delta\ddot{\eta} + \Omega\dot{\eta}) + \Delta\hat{R}(I\ddot{\eta} + \Delta\dot{\eta} + \Omega\eta) + A^T\dot{v} - \Delta A^T v \tag{17}$$

Finally, substituting Eq. (17) into Eq. (14a) gives

$$\hat{R}\,\ddddot{\eta} + (2\Omega\hat{R} - \hat{Q}_v - \hat{R}\Delta^2)\ddot{\eta} + (\hat{R}\Omega^2 + \hat{Q}_d)\eta - (A^T\ddot{v} - \Delta A^T\dot{v} + \Omega A^T v) = 0 \tag{18}$$

Equation (18) represents the set of conditions required for optimal attenuation. For fully actuated systems ($n_a = n_m$), the last bracketed term in Eq. (18) is absent and modal variables η become uncoupled (uncoupled optimality equations were dealt with in [21,22]). For underactuated systems, the n_m equations in set (18) contain n_m modal variables (n_a independent variables η_a and n_r redundant variables η_c) and n_r unknown Lagrange multipliers. To solve for all $n_m + n_r$ unknown functions in vectors η and v, Eq. (18) must be augmented by n_r equations of constraints (9). These constraints, after substituting Eq. (5), take the following differential form in terms of modal variables:

$$AU = A(I\ddot{\eta} + \Delta\dot{\eta} + \Omega\eta) = 0 \tag{19}$$

The modal variables in Eq. (19) are coupled by higher time derivatives. Unlike the independent and redundant components of controls U, related via Eq. (9), the independent components of modal variables η_a cannot be separated analytically from the redundant components of η_c. Therefore, the constraints (19) are nonholonomic.

The set of $n_m + n_r$ equations in Eqs. (18) and (19) contain n_m modal variables in vector η and n_r Lagrange multipliers in vector v. All $n_m + n_r$ unknown functions can be determined provided that $4n_m$ boundary conditions, imposed on n_m components of vector η, are available. Formally, only the independent modes are required to determine the actuation forces (from $F_a = \bar{B}_a(I\ddot{\eta}_a + \Delta\dot{\eta}_a + \Omega\eta_a)$), whereas all the modes are needed to determine any particular DOF (from $X = \phi\eta$). The details of the solution method are discussed in Sec. IV.

Note that the system's constraints (19) resulting from underactuation will always be met in the CMSOC approach, and that the actuators are forced to control all the modes involved. Also, the paths that are specified by the end points will be determined automatically from Eqs. (18) and (19). This problem is somewhat different than solving the problems of controlling underactuated systems to follow the assumed paths (that may or may not satisfy the system's constraints) as presented in [23,24].

IV. Solution Method

Using the symbolic differential operator $D^n = d^n/dt^n$, Eq. (18) can be written as follows:

$$E_i\eta_i = \sum_{j=1}^{n_r} \hat{D}_{ij} v_j, \qquad i = 1 \ldots n_m \tag{20}$$

where

$$E_i = c\omega_i^{-2}D^4 + [2c(1 - 2\zeta_i^2) - b]D^2 + (c + a)\omega_i^2$$

$$\hat{D}_{ij} = a_{ji}(D^2 - 2\zeta_i\omega_i D + \omega_i^2)$$

In turn, Eq. (19) becomes

$$\sum_{i=1}^{n_m} \tilde{D}_{ij}\eta_i = 0 \qquad j = 1 \cdots n_r \tag{21}$$

where

$$\tilde{D}_{ij} = a_{ji}(D^2 + 2\xi_i\omega_i D + \omega_i^2)$$

Operators E_i are of the fourth order, whereas operators $\hat{D}_{ij}$ and $\tilde{D}_{ij}$ are of the second order. The set of Eqs. (20) and (21) can be written in the following matrix form:

$$\underbrace{\begin{bmatrix} E_1 & \cdots & 0 & -\hat{D}_{11} & \cdots & -\hat{D}_{1n_r} \\ \cdots & \cdots & \cdots & \cdots & \cdots & \cdots \\ 0 & \cdots & E_{n_m} & -\hat{D}_{n_m 1} & \cdots & -\hat{D}_{n_m n_r} \\ \tilde{D}_{11} & \cdots & \tilde{D}_{n_m 1} & 0 & \cdots & 0 \\ \cdots & \cdots & \cdots & \cdots & \cdots & \cdots \\ \tilde{D}_{1n_r} & \cdots & \tilde{D}_{n_m n_r} & 0 & \cdots & 0 \end{bmatrix}}_{\bar{E}} \underbrace{\begin{bmatrix} \eta_1 \\ \cdots \\ \eta_{n_m} \\ v_1 \\ \cdots \\ v_{n_c} \end{bmatrix}}_{Y} = \bar{E}Y = 0 \tag{22}$$

Matrix $\bar{E}$ is of size $n_t = n_r + n_m$, and vector Y contains all the unknown modal variables and Lagrange multipliers. Each component of Y in Eq. (22) must satisfy the following condition:

$$\det \bar{E} \cdot Y_i = \tilde{E} \cdot Y_i = 0 \tag{23}$$

Operator $\tilde{E} = \det \bar{E}$ can always be found for known operators E_i, $\hat{D}_{ij}$, and $\tilde{D}_{ij}$. Conveniently, Eq. (23) can be solved by symbolic mathematical software. The MAPLE program was used in the examples to follow.

Note that in Eq. (22) the upper-left portion of matrix $\bar{E}$ is diagonal, whereas the lower right portion consists of zero terms. Consequently, the order of $\tilde{E}$ is always $4n_m$ (i.e., $\tilde{E} = D^{4n_m} + \cdots$), independent of the number of Lagrange multipliers. For example, the explicit forms of this operator for a few selected cases with different numbers of n_m modes and n_a actuators are

$$\tilde{E} = E_1\hat{D}_{21}\tilde{D}_{21} + E_2\hat{D}_{11}\tilde{D}_{11} \qquad n_m = 2 \quad \text{and} \quad n_a = 1$$

$$\tilde{E} = E_1\hat{D}_{21}\tilde{D}_{21}\hat{D}_{32}\tilde{D}_{32} + E_2\hat{D}_{11}\tilde{D}_{11}\hat{D}_{32}\tilde{D}_{32} + E_3\hat{D}_{11}\tilde{D}_{11}\hat{D}_{22}\tilde{D}_{22}, \qquad n_m = 3 \quad \text{and} \quad n_a = 1$$

$$\tilde{E} = E_1E_2E_4\hat{D}_{31}\tilde{D}_{31} + E_1E_3E_4\hat{D}_{21}\tilde{D}_{21} + E_2E_3E_4\hat{D}_{11}\tilde{D}_{11}, \qquad n_m = 4 \quad \text{and} \quad n_a = 3$$

Each term in $\tilde{E}$ is a product of n_a operators E_i and n_r pairs $\hat{D}_{ij}\tilde{D}_{ij}$ ($n_r = n_m - n_a$). For fully actuated problems, for which $n_c = 0$ (all $a_{ij} = 0$), operator $\tilde{E}$ becomes

$$\tilde{E} = E_1 \cdot E_2 \cdots E_{n_m} = 0 \tag{24}$$

Once $\tilde{E}$ in Eq. (23) is determined, the corresponding characteristic equation can be obtained by substituting $D^n \to r^n$ to obtain a $4n_m^{\text{th}}$-order polynomial in the form $r^{4n_m} + \cdots = 0$. The roots of this polynomial are $r_k = \pm\alpha_k \pm i\beta_k$ ($k = 1, \ldots, n_m$), where α_k and β_k are real nonnegative numbers. The general solution to each of the unknown functions Y_j in Eq. (22) consists of the superposition of $4n_m$ exponential functions with complex exponents r_k. For example, if α_k and β_k are nonmultiple, then for any Y_j four independent solving functions are generated in the following form:

$$e^{-\alpha_k t}(c_{kj}^1 \sin\beta_k t + c_{kj}^2 \cos\beta_k t) \quad \text{and} \quad e^{+\alpha_k t}(c_{kj}^3 \sin\beta_k t + c_{kj}^4 \cos\beta_k t) \tag{25}$$

The unknown integration constants $c_{kj}^1, \ldots, c_{kj}^4$, which are discussed in more detail in the Appendix, are $4n_m n_t$ in total. These additional constants must be chosen such that each generated solution Y_j satisfies the original Eqs. (18) and (19). This can be secured by directly substituting and comparing the terms of similar solving functions in these equations, which yields $4n_m n_t$ *additional* linear algebraic equations, $4n_m n_m$ from Eq. (18) and $4n_m n_r$ from Eq. (19).

Any set of $4n_m$ linear algebraic equations, obtained from one differential equation in Eq. (18) or Eq. (19), must be replaced by a set of $4n_m$ equations representing the initial and final boundary conditions for the modal variable vector η to obtain a complete set of linearly independent algebraic equations. Conveniently, all the required $4n_m n_t$ integration constants can be determined automatically from the MAPLE program.

Any disturbances may be assumed in the form of the initial conditions $X(0) = X_0$ and $\dot{X}(0) = \dot{X}_0$. These conditions can be converted into initial conditions for the modal variables by applying Eqs. (4a) and (3a) to obtain

$$\eta(0) = \tilde{\phi}^T M X(0) = \eta_0 \qquad \dot{\eta}(0) = \tilde{\phi}^T M \dot{X}(0) = \dot{\eta}_0 \tag{26}$$

To represent the system at rest, with vibrations eliminated, the final conditions take the following form:

$$X(\infty) = \dot{X}(\infty) = 0 \quad \text{or} \quad \eta(\infty) = \dot{\eta}(\infty) = 0 \tag{27}$$

Equations (27) assume an infinite maneuver time, which is routinely done to formulate the so-called time-invariant control problems. Constants c_{kj}^3 and c_{kj}^4 in Eq. (25) must be zero for such problems due to conditions (27). Therefore, the solutions to Eqs. (23) take the following form:

$$Y_j = \sum_{k=1}^{n_m} e^{-\alpha_k t}(c_{kj}^1 \sin\beta_k t + c_{kj}^2 \cos\beta_k t) \qquad j = 1 \cdots n_t \tag{28}$$

where Y_j represents either η_j or v_j. Now only $2n_m n_t$ integration constants c_{kj}^1 and c_{kj}^2 are to be determined. Parameters β_k and α_k can, respectively, be interpreted as the frequency and active damping associated with the kth controlled mode. Any vibrations with the frequency β_k will be reduced to about 3% of the initial value after $\alpha_k t_k^{\text{ef}} \geq 3.5$, where t_k^{ef} denotes an "effective" settling time for this particular frequency (i.e., $t_i^{\text{ef}} \cong 3.5/\alpha_i$). Also, the active damping ratio of the kth mode is defined as $\xi_k = \alpha_k/\beta_k$. However, because the modes are coupled, the values of α_k or t_k^{ef} better characterize the attenuation of a particular mode than the value of ξ_k.

The complete CMSOC procedure requires some interaction between the FE software (ANSYS) and the symbolic math software (MAPLE). The ANSYS program provides the characteristic parameters of the mechanical system (ω_i, ϕ_i) and the terms of matrix A (for simpler structures, these parameters may be determined analytically). Next, MAPLE determines operator $\tilde{E} = \det \bar{E}$, solves for the roots of its characteristic equation, and generates the corresponding solution functions (28). These functions are substituted back into Eqs. (18) and (19) to group the coefficients of similar terms to obtain the set of *additional* equations, which together with the boundary conditions (26) and (27) determine the complete set of required integration constants and modal variable vector η (more details are given in the Appendix).

Optimal modal control vector U (with independent and redundant components) is obtained by substituting modal variables into Eq. (5), whereas actuation forces are obtained from Eq. (11). Finally, the trajectory of any DOF of interest can be determined from Eq. (4a). This way, the process of optimally controlling vibrations can be fully simulated starting from any assumed set of disturbances to the configuration at rest. More details of this procedure are presented in the numerical examples.

Also, it can be shown that the actuation forces in the CMSOC method can be expressed as a function of the state variables:

$$F_a = -G \cdot \begin{bmatrix} \eta \\ \dot{\eta} \end{bmatrix} \tag{29}$$

where the terms of the gain matrix G of size $n_a \times 2n_m$ can be determined by comparing similar functions defining the forces and the state, similar to how it was done for fully actuated systems in [22]. The details of determining matrix G are not discussed further in this paper.

Note that, for fully actuated systems, operator (24) is a series of independent fourth order operators E_i, where $i = 1 \cdots n_m$. Thus, *additional* differentiations are avoided and, consequently, no *additional* integration constants are generated. Solving each equation $E_i = 0$ leads to four integration constants to be obtained directly from four boundary conditions (26) and (27) for the ith mode. This confirms that in the CMSOC procedure the modal variables of fully actuated problems can be solved independently, one by one, as in the IMSC approach [19]).

V. Example I: Discrete Two-Mass Suspension Problem

The first numerical example is a simple *discrete* two-mass problem, which is presented to familiarize the reader with the basic steps of the procedure. Most of the operations for this problem can be recreated without using computer software.

The discrete underactuated system with two DOF [two modes of vibration ($n_m = 2$)] and controlled by a single actuator ($n_a = 1$,

$n_r = 1$), is shown in Fig. 1. The system has been used to rudimentarily represent the active suspension of a car [16], and so it will be referred to as the suspension problem.

A quarter of the car's mass is denoted by m_2, and the mass of one wheel with attachments is denoted by m_1. The tire stiffness is represented by k_1, and the stiffness of a spring in the shock absorber is represented by k_2 (typically $m_2 \gg m_1$ and $k_2 \ll k_1$). F_a represents the real actuator force, and $F_d = 0$ is a dummy actuator's force [these two actuators ensure the nonsingularity of matrix $\hat{B}$ in Eq. (8)].

The matrices and the nodal force vectors, as defined in Eq. (1), are

$$M = \begin{bmatrix} m_1 & \\ & m_2 \end{bmatrix} \quad K = \begin{bmatrix} k_1 + k_2 & -k_2 \\ -k_2 & k_2 \end{bmatrix} \quad F = \begin{bmatrix} -1 & 1 \\ 1 & 0 \end{bmatrix} \begin{bmatrix} F_a \\ F_d \end{bmatrix}$$

The following numerical values are assumed for the analysis:

$$m_1 = 40\,\text{kg} \quad m_2 = 200\,\text{kg} \quad k_1 = 235.4\,\text{kN/m} \quad k_2 = 39.24\,\text{kN/m}$$

Modal analysis renders the following frequencies of free vibrations and modal shape matrix:

$$\omega_1 = 12.94\ \text{rad/s} \qquad \omega_2 = 83.04\ \text{rad/s} \tag{30a}$$

$$\phi = \tilde{\phi} = \begin{bmatrix} 0.01033 & 0.15778 \\ 0.07056 & -0.00462 \end{bmatrix} \tag{30b}$$

Initially the system is at rest in the position $x_1(0) = 4$ mm and $x_2(0) = 5$ mm. The corresponding four boundary conditions for the modal variables are

$$\eta_1(0) = 0.07221 \qquad \eta_2(0) = 0.02062 \tag{31a}$$

$$\dot{\eta}_1(0) = 0 \qquad \dot{\eta}_2(0) = 0 \tag{31b}$$

For actuators F_a and F_d, matrix $\hat{B}'$ in Eq. (8) is

$$\hat{B}' = \tilde{\phi}^T B = \begin{bmatrix} 0.01033 & 0.07056 \\ 0.1578 & -0.004620 \end{bmatrix} \begin{bmatrix} -1 & 1 \\ 1 & 0 \end{bmatrix} = \begin{bmatrix} 0.06023 & 0.01033 \\ -0.1624 & 0.1578 \end{bmatrix}$$

Applying Eq. (8) yields

$$\begin{bmatrix} F_a \\ F_d \end{bmatrix} = (\hat{B}')^{-1} U = \begin{bmatrix} \tilde{B}_a & \tilde{B}_r \\ A_a & A_r \end{bmatrix} \begin{bmatrix} U_a \\ U_r \end{bmatrix} = \begin{bmatrix} 14.11 & -0.9241 \\ 14.53 & 5.387 \end{bmatrix} \begin{bmatrix} u_1 \\ u_2 \end{bmatrix} = \begin{bmatrix} F_a \\ 0 \end{bmatrix}$$

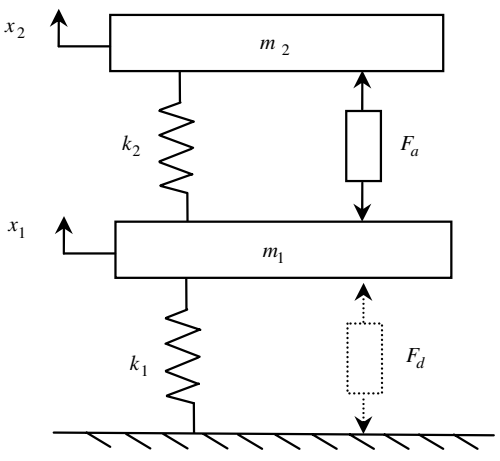

Fig. 1 Suspension system.

The second row of this operation gives the constraint matrix ($A = [\,14.53 \quad 5.387\,]$), which can be normalized according to Eq. (10) to render

$$A = [\,1 \quad 0.3709\,] \tag{32}$$

The elements of this matrix are denoted as $a_{11} = 1$ and $a_{12} = 0.3709$. Note the latter term represents a one-term matrix A_r.

The actuator force may be written according to Eq. (11) in the following form:

$$F_a = 16.60 u_1 \tag{33}$$

This equation reflects the relationship between the actuator force and the independent modal control [the numerical value 16.60 represents a one-term matrix $\bar{B}_a$ in Eq. (11)].

It can easily be verified that identical A and $\bar{B}_a$ will be obtained if the dummy actuator is positioned, for example, between mass m_2 and the ground.

The controllability parameters, given by Eqs. (12a) and (12b), are

$$\lambda = 0.3709 \qquad \kappa = 16.60 \tag{34}$$

These parameters are of limited interest in this problem, as the number of possible single-actuator configurations is small, but they are shown here for completeness. The next example, in Sec. VI, will discuss them in greater detail.

The assumed optimization parameters in the performance index (2) are $a = b = c = 1$, making the diagonal weighting matrices in the modal performance index (6) equal to

$$\hat{Q}_{dii} = \omega_i^2 \qquad \hat{Q}_{vii} = 1 \qquad \hat{R}_{ii} = 1/\omega_i^2$$

Operators given by Eqs. (20) and (21) take the following form:

$$E_i = D^4 \omega_i^{-2} + D^2 + 2\omega_i^2 \quad \text{and} \quad \hat{D}_{ij} = \tilde{D}_{ij} = a_{ji}(D^2 + \omega_i^2)$$

Substituting into Eq. (22) and solving for $\tilde{E}$ in Eq. (23), we obtain the eighth-order operator

$$\tilde{E} = \tilde{D}_{11}^2 E_2 + \tilde{D}_{12}^2 E_1$$

The roots of this characteristic equation are $r_k = \pm\alpha_k \pm i\beta_k$ ($k = 1, 2$), where

$$\alpha_1 = 7.574 \qquad \alpha_2 = 22.36 \qquad \beta_1 = 12.82 \qquad \beta_2 = 82.87 \tag{35}$$

Note that $\beta_i \cong \omega_i$. Also note that for this case $\alpha_2 \approx 3\alpha_1$, indicating that the second frequency will be eliminated at a faster rate than the first (the modal active damping ratios formally are $\xi_1 = 0.5909$ and $\xi_2 = 0.2722$).

For the time-invariant problem, each unknown variable contains four independent terms (each term corresponding to a distinct root of the characteristic equation) and four integration constants. Unknown modal variables $\eta_1 = Y_1$, $\eta_2 = Y_2$, and Lagrange multiplier $v_1 = Y_3$ thus take the form [see (28)]

$$Y_j = e^{-\alpha_1 t}[c_{1j}^1 \sin(\beta_1 t) + c_{1j}^2 \cos(\beta_1 t)] + e^{-\alpha_2 t}[c_{2j}^1 \sin(\beta_2 t) + c_{2j}^2 \cos(\beta_2 t)] \tag{36}$$

In total, there are 12 integration constants, c_{1j}^1, c_{2j}^1, c_{1j}^2, and c_{2j}^2 ($j = 1, 2, 3$), needed to describe η_1, η_2, and v_1. To find their numerical values, an equal number of independent algebraic equations are required. These equations are generated as follows.

For this problem, the optimality equation (18) is ($n_m = 2$)

$$\dddot{\eta}_i + \omega_i^2 \ddot{\eta}_i + 2\omega_i^4 \eta_i = a_{1i}\omega_i^2(\ddot{v} + \omega_i^2 v) \qquad i = 1, 2 \tag{37}$$

The nonholonomic constraint (19) is ($n_r = 1$)

$$a_{11}(\ddot{\eta}_1 + \omega_1^2 \eta_1) + a_{12}(\ddot{\eta}_2 + \omega_2^2 \eta_2) = 0 \tag{38}$$

Substituting η_1, η_2, and v_1 [in the form of Eq. (36)] into Eqs. (37) and (38) and comparing similar terms yields $n_t = n_m + \eta_r = 3$ sets of homogeneous linear equations (with constants c_{kj}^l as unknowns), each set containing $2n_m = 4$ algebraic equations, which all together yields 12 homogeneous linear equations. A nontrivial solution for c_{kj}^l is obtained by ignoring one set of equations [either from Eq. (37) or Eq. (38)] and replacing it with the set of initial boundary conditions (31a).

The calculated integration constants for the suspension problem [see (A1)] are substituted back into Eq. (36) to obtain the modal variables, which are plotted in Figs. 2a and 2b. Both frequencies, with the periods $T_1 = 0.49$ s and $T_2 = 0.076$ s, contribute to the response of each modal variable; this is particularly visible for the second modal variable in Figs. 2a and 2b.

The histograms of the DOF are plotted in Figs. 3a and 3b, in which it appears that x_1 is dominated by the second frequency and x_2 is dominated by the first frequency. The second frequency oscillations disappear faster than oscillations with the first frequency, because $\alpha_2 > \alpha_1$. The settling times (i.e., $t_i^{\text{ef}} \cong 3.5/\alpha_i$) are $t_1^{\text{ef}} = 0.462$ s and $t_2^{\text{ef}} = 0.156$ s, which is apparent in Figs. 2–5.

The modal controls, plotted in Fig. 4, satisfy the constraint equation $AU = 0$ [where A is given in Eq. (32)] or, according to Eq. (9), $h(u_1, u_2) = u_1 + 0.3709u_2 = 0$.

The actuation force to control this 2-DOF system is obtained from Eq. (33) and plotted in Fig. 5. The maximum required actuation force is about 270 N. Note how the frequencies of both participating modes affect its variation in time (though for $t > t_2^{\text{ef}}$ only the frequency of the first mode is significant in the variation of F_a).

VI. Example II: Distributed-Mass Frame Problem

The second example is a continuous system that requires the use of both FE and symbolic mathematics programs. The main purpose of this example is to demonstrate the abilities of the CMSOC procedure to predict the performance of particular configurations of the actuators in the FE phase of simulation. These predictions are then verified in the control phase. Special attention will be paid to the relationship between the magnitudes of the parameters of controllability, λ and κ, determined at the beginning of the simulation, and the response characteristics of the controlled system. In particular,

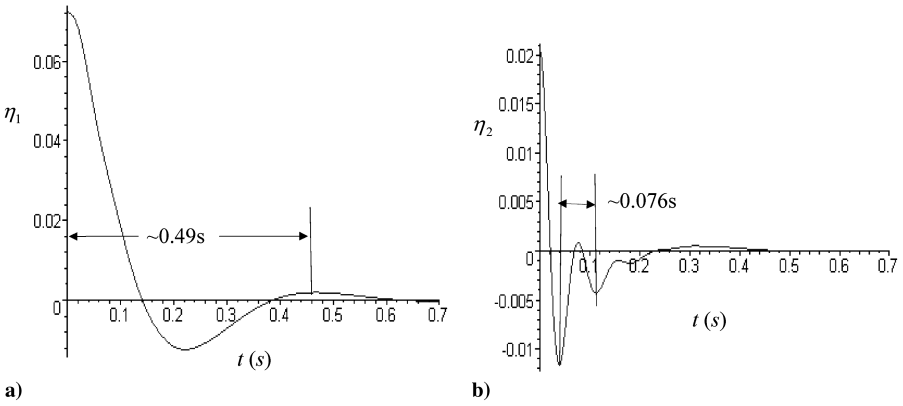

a) b)

Fig. 2 Modal variables as a function of time: a) η_1, and b) η_2.

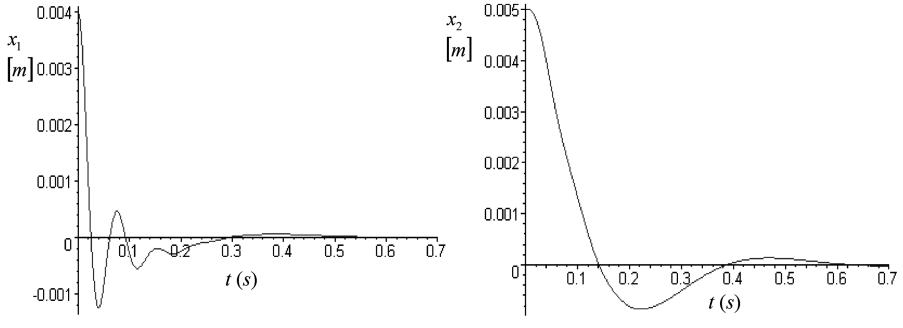

a) b)

Fig. 3 Position of DOF as a function of time: a) x_1, and b) x_2.

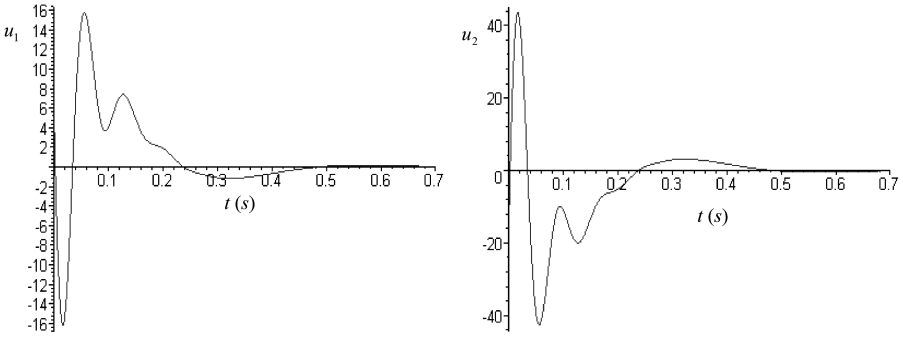

a) b)

Fig. 4 Modal controls as a function of time: a) u_1, and b) u_2.

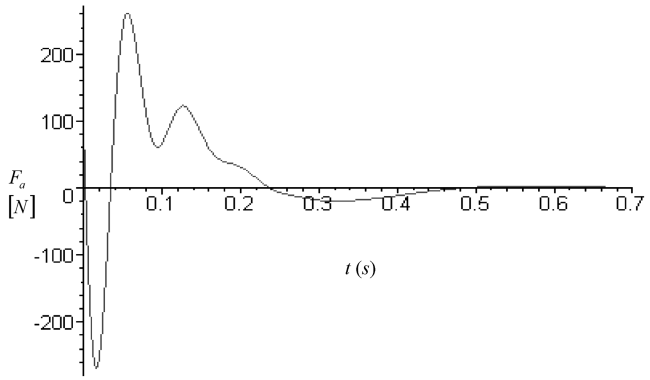

Fig. 5 Optimal actuation force F_a as a function of time.

note how either excessively long attenuation times (case 4) or excessively large actuation force requirements (case 6) can be identified from these parameters.

A distributed-mass three-stage plane frame is shown in Fig. 6a. All members are aluminum ($E = 71.7$ GPa, $\rho = 2800$ kg/m^3) with a cross-sectional area of 76 mm^2 (a mass of 0.2128 kg/m) and an area moment of inertia of 4585 mm^4. The topmost horizontal member weighs 1 kg and is considered rigid.

The frame was modeled in ANSYS by two-dimensional beam (five elements per member) and mass elements as a 120-DOF system. The locations of all relevant nodes are indicated in the figure. The horizontal and vertical displacements at node p are denoted by d_x^p and d_y^p, respectively. The modal shapes of the four lowest vibration modes, with frequencies ω_i ($i = 1 \cdots 4$), are shown in Fig. 6b. The attenuation of disturbance in the frame will be simulated for several different numbers and configurations of actuators that actively control three or four modes of vibrations. Actuators exert equal and opposite axial forces along a line between any two points on the frame where they are attached.

The actuator configurations as well as the number of modes n_m that will be considered are indicated in Fig. 7. As mentioned, the focus of this example is on the assessment and improvement of attenuation performance through actuator configuration, and so in each case in Fig. 7 the controllability parameters, λ and κ, will be of particular interest. Note that nearly all cases can be analyzed by using the same matrix $\hat{B}$ for the system, but differently assigning the actuators as real and dummy. This indicates that the locations of dummy actuators, though arbitrary, should be selected in the analysis in such a way that, in searching for improved performance, they potentially may be switched with the real ones.

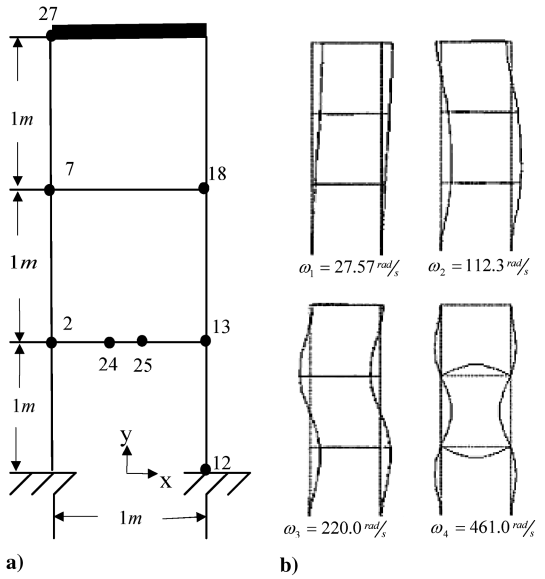

Fig. 6 Shown are the following: a) the frame, and b) its first four modal shapes and frequencies.

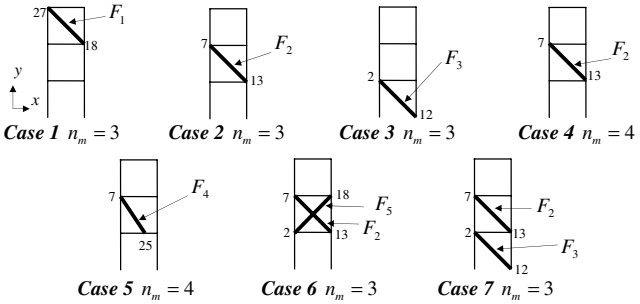

Fig. 7 Actuator configurations and number of modes n_m to be considered.

An initial disturbance is assumed in terms of modal variables as

$$\begin{aligned} &\eta_1(0) = 0.05 \qquad \eta_3(0) = 0.0045 \qquad \dot{\eta}_i(0) = 0 \\ &\eta_2(0) = 0.005 \qquad \eta_4(0) = 0.004 \qquad i = 1 \cdots 4 \end{aligned} \tag{39}$$

Conditions (39), when mapped into the DOF space, correspond to the initial displacements:

$$d_x^{27} = 0.03801 \text{ m} \qquad d_x^{7} = 0.02838 \text{ m} \qquad d_y^{24} = -0.005740 \text{ m} \tag{40}$$

As in the first example, the assumed optimization parameters in the performance index (2) are $a = b = c = 1$. The modal analysis for this problem was performed using the ANSYS software.

Upon inspection of the modal shapes in Fig. 6, it may be concluded that one actuator attached at corner nodes, as in cases 1–3, should be able to control the first three vibration modes reasonably well. However, some difficulty might be expected when trying to control the fourth vibration mode shape in all cases (with the exception of case 5), as the actuators are located at almost stationary corner nodes of the fourth mode. This will be demonstrated in case 4, in which the actuator from case 2 is used to control all four modes. The actuator in case 5 should control the fourth mode better, due to its slightly shifted location away from the corner nodes. Case 6 offers another example of poor actuator positioning for controlling three modes of vibration, but for a somewhat more complicated reason. The configuration in case 7, which "combines" cases 2 and 3, should significantly improve the control over case 6. These somewhat intuitive observations are to be verified by the method proposed by performing the following simulations.

A. Case 1 Actuator F_1 to Control Three Modes

The first three modes of vibration are to be controlled by actuator F_1 located between nodes 18 and 27 ($n_a = 1$, $n_m = 3$, $n_r = 2$, and $n_t = 5$). If F_2 and F_3 (between nodes 7 and 13 and 2 and 12, respectively) are selected as dummy actuators, then Eq. (8) takes the following form (all the numbers were obtained from the ANSYS modal analysis):

$$\begin{aligned} \begin{bmatrix} F_a \\ F_d \end{bmatrix} &= (\hat{B}')^{-1} U = \begin{bmatrix} \tilde{B}_a & \tilde{B}_r \\ A_a & A_r \end{bmatrix} \begin{bmatrix} U_a \\ U_r \end{bmatrix} \\ &= \begin{bmatrix} -1.341 & 0.6895 & -0.3246 \\ -1.871 & 0.1265 & 0.3834 \\ -2.097 & -0.6688 & -0.2668 \end{bmatrix} \begin{bmatrix} u_1 \\ u_2 \\ u_3 \end{bmatrix} = \begin{bmatrix} F_1 \\ 0 \\ 0 \end{bmatrix} \end{aligned} \tag{41}$$

The lower partition (two bottom rows) of Eq. (41) forms the constraint matrix, that when normalized to the form defined in Eq. (10) becomes

$$A = \begin{bmatrix} 1 & 0.1708 & \\ & 1 & 0.8592 \end{bmatrix} \tag{42}$$

According to Eq. (11), the actuation force can be expressed as

$$F_1 = \bar{B}_a U_a = -7.588 u_1 \tag{43}$$

The controllability parameters, given by (12a) and (12b), are

$$\lambda = 0.1468 \qquad \kappa = 7.588 \tag{44}$$

Recall that rate indicator λ should have a value "close" to unity, indicating that a given actuator configuration can quickly attenuate all controlled modes. Also, the effort parameter should have a "small" value, so that the actuator in this configuration will have small maximum force requirements. The meanings of close and small are relative and will be clarified later in this section.

The explicit forms of the optimality and constraint Eqs. (18) and (19) are

$$\dddot{\eta}_i + \omega_i^2 \ddot{\eta}_i + 2\omega_i^4 \eta_i = a_{1i}\omega_i^2(\ddot{v}_1 + \omega_i^2 v_1) + a_{2i}\omega_i^2(\ddot{v}_2 + \omega_i^2 v_2) \qquad i = 1, 2, 3 \tag{45a}$$

$$a_{j1}(\ddot{\eta}_1 + \omega_1^2\eta_1) + a_{j2}(\ddot{\eta}_2 + \omega_2^2\eta_2) + a_{j3}(\ddot{\eta}_2 + \omega_2^2\eta_2) = 0 \qquad j = 1, 2 \tag{45b}$$

The roots of the characteristic equation ($r_k = \pm\alpha_k \pm i\beta_k$), given by Eq. (23), are calculated as

$$\alpha_1 = 7.308 \qquad \alpha_2 = 50.44 \qquad \alpha_3 = 62.20$$
$$\beta_1 = 27.68 \qquad \beta_2 = 116.6 \qquad \beta_3 = 213.7 \tag{46}$$

Note that again $\beta_i \approx \omega_i$. The corresponding modal active damping ratios are $\xi_1 = 0.2640$, $\xi_2 = 0.4324$, and $\xi_3 = 0.2911$, and the effective settling times for the three controlled modes are

$$t_1^{\text{eff}} = 0.4789 \text{ s} \qquad t_2^{\text{eff}} = 0.06939 \text{ s} \qquad t_3^{\text{eff}} = 0.05627 \text{ s} \tag{47}$$

These settling times are reflected in Fig. 8, in which oscillations with the second and third frequencies disappear after about 0.07 s, and those with the first frequency after about 0.48 s.

Solving for the unknown 30 constants ($2n_m n_t$, see comments in the Appendix) enables the determination of all modal variables, modal controls, actuation force, and the response of any DOF of interest. Plots of some of these variables are shown in Fig. 8.

The uncontrolled fourth modal variable, given by $\eta_4(t) = \eta_4(0)\cos(\omega_4 t)$, is not shown. However, it is included in the DOF responses, d_x^{27}, d_x^7, and d_y^{24}. Because of its shape, the fourth mode (see Fig. 6), which is unattenuated, hardly affects horizontal displacements d_x^{27} and d_x^7 (Fig. 8h), but significantly impacts vertical displacement d_y^{24} (Fig. 8i). Actuation force F_1 has a peak value of 130.7 N (see Fig. 8g).

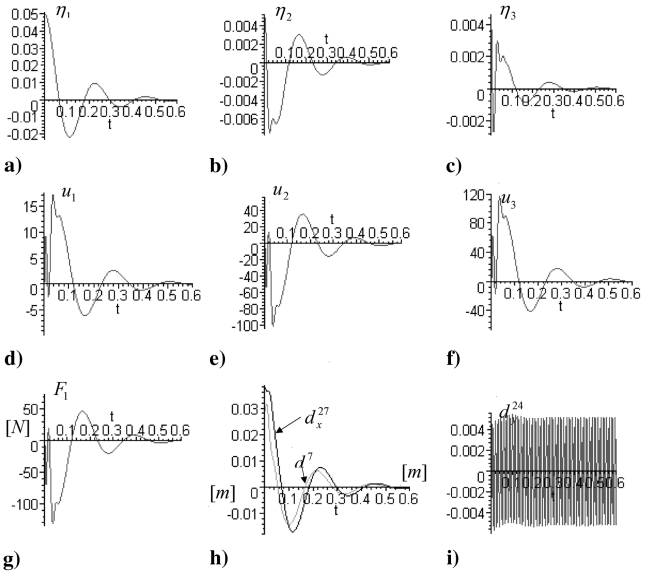

Fig. 8 Histograms for case 1: a, b, c) of modal variables; d, e, f) modal controls; g) actuation force; and h, i) displacements.

B. Case 2 Actuator F_2 to Control Three Modes

The first three modes of vibration are to be controlled by actuator F_2 located between nodes 7 and 13 ($n_a = 1$, $n_m = 3$, $n_r = 2$, and $n_t = 5$). For this case, F_1 and F_3 may be considered dummy actuators; hence, Eq. (8) is identical to that used in case 1 [given in Eq. (41)], only the first and second rows of $(\hat{B}')^{-1}$ are swapped, rendering

$$\begin{bmatrix} F_a \\ F_d \end{bmatrix} = (\hat{B}')^{-1}U = \begin{bmatrix} \tilde{B}_a & \tilde{B}_r \\ A_a & A_r \end{bmatrix}\begin{bmatrix} U_a \\ U_r \end{bmatrix} = \begin{bmatrix} -1.871 & 0.1225 & 0.3834 \\ -1.341 & 0.6895 & -0.3246 \\ -2.097 & -0.6688 & -0.2668 \end{bmatrix}\begin{bmatrix} u_1 \\ u_2 \\ u_3 \end{bmatrix} = \begin{bmatrix} F_2 \\ 0 \\ 0 \end{bmatrix} \tag{48}$$

By partitioning form (48), the pseudotransfer matrix and constraint matrix are calculated by Eqs. (10) and (11), respectively, to obtain

$$\bar{B}_a = -4.212 \qquad A = \begin{bmatrix} 1 & 1.242 & \\ & 1 & -0.1379 \end{bmatrix} \tag{49}$$

The controllability parameters from (12a) and (12b) are

$$\lambda = 0.1713 \qquad \kappa = 4.212 \tag{50}$$

Rate parameter λ is slightly closer to unity, reflecting a marginal improvement in the attenuation rate of the slowest mode. Also, effort parameter κ in Eq. (50) is slightly lower than in case 1, and so a slightly smaller maximum force should be expected. In fact, as shown in Fig. 9b, the actuation force F_2 has a peak value of 121.0 N, in comparison with $F_1^{\max} = 130.7$.

The roots ($r_k = \pm\alpha_k \pm i\beta_k$) of Eq. (23) are

$$\alpha_1 = 12.91 \qquad \alpha_2 = 9.260 \qquad \alpha_3 = 88.65$$
$$\beta_1 = 27.51 \qquad \beta_2 = 112.6 \qquad \beta_3 = 218.7 \tag{51}$$

The effective settling times are

$$t_1^{\text{eff}} = 0.2712 \text{ s} \qquad t_2^{\text{eff}} = 0.3780 \text{ s} \qquad t_3^{\text{eff}} = 0.03950 \text{ s} \tag{52}$$

C. Case 3 Actuator F_3 to Control Three Modes

Now consider controlling the frame's first three modes of vibration with actuator F_3, located between nodes 2 and 12. For this case, F_1 and F_2 may be considered dummy actuators and so Eq. (8) is also identical to case 1 [given in Eq. (41)], with the first and third rows of $(\hat{B}')^{-1}$ swapped, giving

$$\begin{bmatrix} F_a \\ F_d \end{bmatrix} = (\hat{B}')^{-1}U = \begin{bmatrix} \tilde{B}_a & \tilde{B}_r \\ A_a & A_r \end{bmatrix}\begin{bmatrix} U_a \\ U_r \end{bmatrix} = \begin{bmatrix} -2.097 & -0.6688 & -0.2668 \\ -1.871 & 0.1265 & 0.3834 \\ -1.341 & 0.6895 & -0.3246 \end{bmatrix}\begin{bmatrix} u_1 \\ u_2 \\ u_3 \end{bmatrix} = \begin{bmatrix} F_3 \\ 0 \\ 0 \end{bmatrix} \tag{53}$$

The pseudotransfer matrix and constraint matrix become

$$\bar{B}_a = -5.532 \qquad A = \begin{bmatrix} 1 & -0.2723 & \\ & 1 & -1.001 \end{bmatrix} \tag{54}$$

The controllability parameters are

$$\lambda = 0.2726 \qquad \kappa = 5.532 \tag{55}$$

Rate parameter λ is again slightly closer to unity than in cases 1 and 2, signaling that a marginal improvement in the slowest attenuation rate is expected. Effort parameter κ is of a similar magnitude to both cases 1 and 2, and so a similar maximum force is expected in this case. Accordingly, the maximum force for actuator F_3 is 131.4 N.

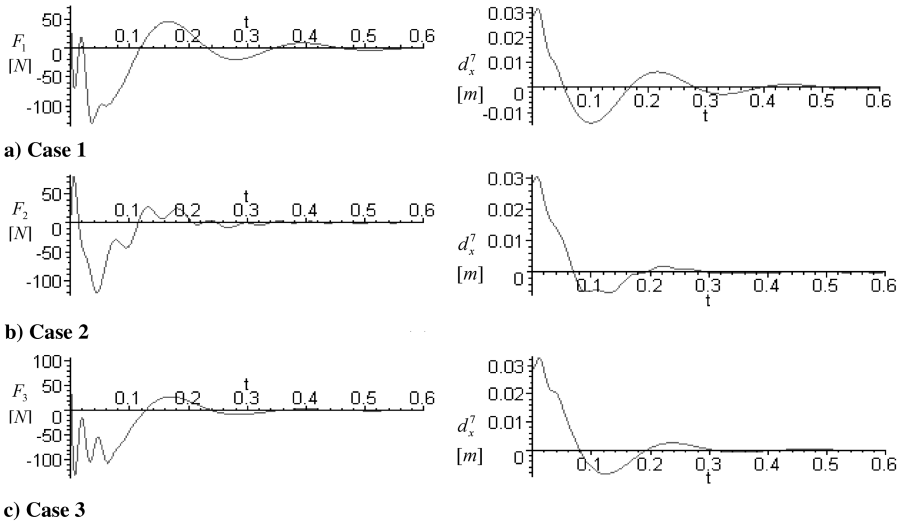

Fig. 9 Cases 1–3: optimal control forces (left) and DOF response (right).

The roots of Eq. (23) are ($r_k = \pm\alpha_k \pm i\beta_k$)

$$\alpha_1 = 10.74 \qquad \alpha_2 = 46.13 \qquad \alpha_3 = 45.56$$
$$\beta_1 = 27.73 \qquad \beta_2 = 114.0 \qquad \beta_3 = 216.9 \tag{56}$$

And the corresponding settling times are

$$t_1^{\text{eff}} = 0.3260 \text{ s} \qquad 0.07670 \text{ s} \qquad t_3^{\text{eff}} = 0.07590 \text{ s} \tag{57}$$

The optimal control forces and the x-displacement response of node 7 (d_x^7) for cases 1–3 are shown in Fig. 9 to compare the control efforts and attenuation rates.

In case 1, the disturbance is eliminated in about 0.47 s, in case 2 it takes about 0.38 s, and in case 3 it takes about 0.33 s. These settling times correlate well with the values of rate parameter λ, which takes a value closer to unity for faster attenuation. In cases 1 and 3, the second and third modes are attenuated quickly (in about 0.07 s), whereas in case 2 the second mode is attenuated last (in about 0.38 s). The control process requires actuation forces of similar magnitudes with the maximum forces of 130.7 N in case 1, 121.0 N in case 2, and 131.4 N in case 3, which is approximately correlated to the effort parameter κ. As can be observed, a single actuator attached diagonally between opposite corner nodes of the frame, as in cases 1–3, has good authority over the first three modes of vibration. In each of these cases the controllability parameters were all of reasonably similar magnitudes. Rate parameter λ varied between 0.1468 and 0.2726, and effort parameter κ varied between 4.212 and 7.588. Note that the nondiagonal terms in matrices A (a_{ij} for $i \neq j$) were close to unity.

D. Case 4 Actuator F_2 to Control Four Modes

As mentioned already, the actuator positions in cases 1–3 should have poor authority over the fourth mode of vibration. To demonstrate this, actuator F_2, attached at corners nodes 7 and 13 as in case 2, will be used to control four modes of vibrations ($n_a = 1$, $n_m = 4$, $n_r = 3$, and $n_t = 7$). One additional dummy actuator, chosen between nodes 2 and 18 (location F_5 in case 5 of Fig. 6b), is included to write Eq. (8) in the following form:

$$\begin{bmatrix} F_a \\ F_d \end{bmatrix} = \begin{bmatrix} \tilde{B}_a & \tilde{B}_r \\ A_a & A_r \end{bmatrix} \begin{bmatrix} U_a \\ U_r \end{bmatrix}$$
$$= \begin{bmatrix} -3.249 & -0.01304 & -0.1868 & 811.7 \\ -1.341 & 0.6895 & -0.3246 & -0.8639 \times 10^{-5} \\ -2.097 & -0.6688 & -0.2668 & -0.2854 \times 10^{-4} \\ -1.378 & -0.1394 & -0.5702 & 811.7 \end{bmatrix} \begin{bmatrix} u_1 \\ u_2 \\ u_3 \\ u_4 \end{bmatrix}$$
$$= \begin{bmatrix} F_2 \\ 0 \\ 0 \\ 0 \end{bmatrix} \tag{58}$$

The constraint matrix [from the lower partition of (58)] is normalized to

$$A = \begin{bmatrix} 1 & 1.242 & 0 & 0 \\ 0 & 1 & -0.1379 & 0 \\ 0 & 0 & 1 & -2296 \end{bmatrix} \tag{59}$$

Note that $|a_{34}| = 2296 \gg 1$, an indication of poor control over the fourth mode. In fact, matrix (59) requires that $u_2 = -0.805u_1$, $u_3 = -5.84u_1$, and $u_4 = -0.00254u_1$, indicating that the effort assigned to the fourth modal control is much lower than that assigned to other modal controls.

Equation (11) for case 4 is unchanged from case 2 [see Eq. (49)] because the matrix reflects changes in the actuator configuration only; thus, it is written as follows:

$$F_a = F_2 = \bar{B}_a U_a = -4.212u_1 \tag{60}$$

The controllability parameters from Eqs. (12a) and (12b) are

$$\lambda = 393.2 \qquad \kappa = 4.212 \tag{61}$$

Rate parameter λ has increased three orders of magnitude from case 2 [see Eq. (50)], indicating a large expected increase in attenuation time. Effort parameter κ remains unchanged (because the same actuator location is used) between cases 2 and 4, which should be reflected in similar expected maximum actuator forces.

The roots ($r_k = \pm\alpha_k \pm i\beta_k$) of the characteristic equation from Eq. (23) are

$$\alpha_1 = 12.91 \quad \alpha_2 = 9.260 \quad \alpha_3 = 88.65 \quad \alpha_4 = 0.03663$$
$$\beta_1 = 27.51 \quad \beta_2 = 112.6 \quad \beta_3 = 218.7 \quad \beta_4 = 461.0 \tag{62}$$

The small value of α_4 indicates that the fourth mode of vibration is attenuated very slowly. The corresponding settling times are

$$t_1^{\text{eff}} = 0.2711 \text{ s} \quad t_2^{\text{eff}} = 0.3780 \text{ s} \quad t_3^{\text{eff}} = 0.03948 \text{ s} \quad t_4^{\text{eff}} = 95.56 \text{ s} \tag{63}$$

Despite the poor attenuation of the fourth mode, the other three modes are attenuated at the same rate as in case 2.

In Figs. 10a and 10b, the response of the frame's DOF, d_x^7 and d_y^{24}, are shown. The horizontal displacement d_x^7 is only slightly affected by the fourth mode due to its location in relation to the modal shape, but the vertical displacement d_y^{24} is very sensitive to this mode and clearly shows poor attenuation of the fourth mode (95.6 s is needed to eliminate these oscillations).

The optimal actuation force histograms shown in Figs. 10c and 10d (note the different time scales) are now dominated by the fourth mode. In fact, after about 0.5 s only vibrations with the fourth natural frequency ($\approx$461.0 rad/s) persist. The maximum force required by actuator F_2 is about 330 N. Figure 10d confirms that the effective settling time is about $t_4^{\text{eff}} = 95.6$ s.

In conclusion, as expected, when control by a single actuator placed between the corner nodes over the fourth mode is attempted, a large value of the rate parameter λ indicates a nearly uncontrollable system. To reduce its value (to the level characterizing the attenuation rate when controlling only the first three modes of vibration, for example), a new configuration of the actuator with better authority over all controlled modes is needed.

E. Case 5 Actuator F_4 to Control Four Modes

Actuator F_4, located between nodes 7 and 25, should intuitively be better suited to control the frame's four modes of vibration. This configuration is only a slight alteration from case 4, with the lower end of the actuator moved to a location two elements away from node 13.

Dummy actuators are chosen as F_1, F_2, and F_3, and so Eq. (8) takes the following form:

$$\begin{bmatrix} F_a \\ F_d \end{bmatrix} = \begin{bmatrix} -1.518\cdot 10^{-3} & -1.537\times 10^{-4} & -6.282\times 10^{-4} & -0.8944 \\ -1.341 & 0.6895 & -0.3246 & 5.472\times 10^{-3} \\ -2.097 & -0.6688 & -0.2668 & -0.02252 \\ -1.870 & 0.1266 & 0.3838 & -0.6715 \end{bmatrix} \times \begin{bmatrix} u_1 \\ u_2 \\ u_3 \\ u_4 \end{bmatrix} = \begin{bmatrix} F_4 \\ 0 \\ 0 \\ 0 \end{bmatrix} \tag{64}$$

The constraint matrix can be written in the normalized form as follows:

$$A = \begin{bmatrix} 1 & 1.490 & & \\ & 1 & -0.1185 & \\ & & 1 & -0.9208 \end{bmatrix} \tag{65}$$

None of the terms in Eq. (65) is much greater than unity, and so the effort assigned to each modal control is much more evenly distributed than in case 4 [see Eq. (59)]. In fact, constraint matrix (65) requires that $u_2 = -0.671u_1$, $u_3 = -5.662u_1$, and $u_4 = -6.149u_1$ (whereas, for case 4, $u_4 = 0.00254$). The actuator force from Eq. (11) is

$$F_a = F_4 = \bar{B}_a U_a = -5.495u_1 \tag{66}$$

The controllability parameters from Eqs. (12a) and (12b) for case 5 are

$$\lambda = 0.1626 \qquad \kappa = 5.495 \tag{67}$$

The rate indicator λ has decreased three orders of magnitude in comparison to case 4 [see Eq. (61)], to a value much closer to unity. In fact, this parameter has a value that would suggest the rate of attenuation is somewhere in between that of cases 1 and 2; this is

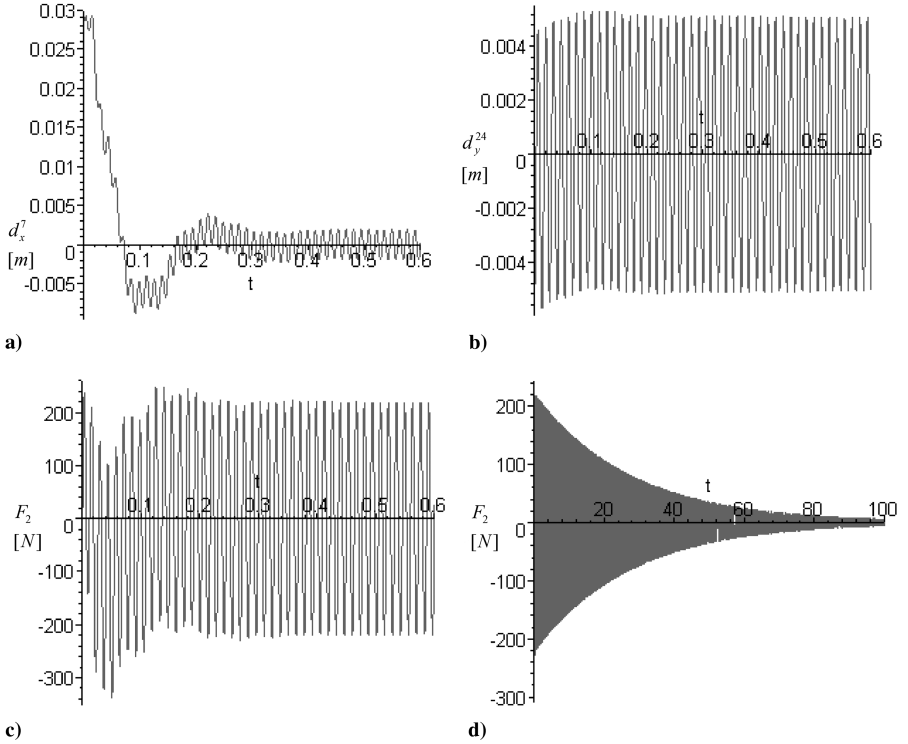

Fig. 10 Case 4: a) response d_x^7; b) response d_y^{24}; and c, d) actuation force F_2.

confirmed in Eqs. (68) and (69). The parameter κ is close in value to previous cases, and so the maximum forces should not be expected to change greatly.

The roots of the characteristic equation, given by Eq. (23), are

$$\alpha_1 = 12.42 \qquad \alpha_2 = 7.484 \qquad \alpha_3 = 78.97 \qquad \alpha_4 = 87.77$$
$$\beta_1 = 27.51 \qquad \beta_2 = 112.5 \qquad \beta_3 = 221.8 \qquad \beta_4 = 457.8 \tag{68}$$

None of the α_i values is small [unlike α_4 in Eq. (62)]; hence, the time required to effectively attenuate each mode of vibration is relatively short. The effective settling times are

$$t_1^{\text{eff}} = 0.2817\ \text{s} \quad t_2^{\text{eff}} = 0.4676\ \text{s} \quad t_3^{\text{eff}} = 0.04432\ \text{s} \quad t_4^{\text{eff}} = 0.03988\ \text{s} \tag{69}$$

The settling times for the first three modes are close in value to case 4 [see Eq. (63)]; however, the fourth mode is now quickly attenuated, in about 0.04 s. Recall that this is achieved by relocating the lower end attachment of actuator F_2 from the corner node 13 to the inner node 25.

The displacements d_x^7 andd_y^{24} are shown in Figs. 11a and 11b, and the actuation force F_4 is shown in Fig. 11c. These plots contrast those of case 4 (Fig. 10), in which the fourth mode was poorly controlled (consequently, d_y^{24} was poorly attenuated). The maximum force needed is about 240 N, and the disturbance is effectively eliminated after $t_2^{\text{eff}} = 0.4676$ s.

F. Case 6 Actuators F_2 and F_5 to Control Three Modes

Two actuators are to control the frame's first three modes of vibration ($n_a = 2$, $n_m = 3$, $n_r = 1$, and $n_t = 4$). Actuator F_2 is located as in case 2, and a second actuator F_5 is located between nodes 2 and 18. With actuator F_1 as a dummy, Eq. (8) becomes

$$\begin{bmatrix} F_a \\ F_d \end{bmatrix} = \begin{bmatrix} -5.968 \times 10^7 & -1.903 \times 10^7 & -7.593 \times 10^6 \\ -5.968 \times 10^7 & -1.903 \times 10^7 & -7.593 \times 10^6 \\ -0.7019 & 0.8942 & -0.2433 \end{bmatrix} \begin{bmatrix} u_1 \\ u_2 \\ u_3 \end{bmatrix} = \begin{bmatrix} F_2 \\ F_5 \\ 0 \end{bmatrix} \tag{70}$$

The normalized constraint matrix (10) is

$$A = [\,1 \quad -1.274 \quad 0.3466\,] \tag{71}$$

No element in this row matrix is significantly greater than unity, suggesting that reasonable attenuation rates are expected.

The actuation forces F_2 and F_5, as defined by Eq. (11), are

$$F_a = \bar{B}_a U_a = \begin{bmatrix} -37,769,742 & -46,942,466 \\ -37,769,738 & -46,942,463 \end{bmatrix} \begin{bmatrix} u_1 \\ u_2 \end{bmatrix} = \begin{bmatrix} F_2 \\ F_5 \end{bmatrix} \tag{72}$$

Now matrix $\bar{B}_a$ contains terms of large magnitudes, indicating that the modal controls will produce large actuation forces. Eight significant digits are shown in Eq. (72) to verify that matrix $\bar{B}_a$ is nearly, but not exactly, singular.

For case 6, the control parameters from Eqs. (12a) and (12b) are

$$\lambda = 0.3466 \qquad \kappa = 74.46 \times 10^6 \tag{73}$$

Rate parameter λ has a value closer to unity than any previous cases, and so the attenuation rate of the slowest mode should be expected to increase; this is confirmed in Eqs. (74) and (75). However, effort parameter κ is seven orders of magnitude larger than previous cases, indicating that the maximum expected forces will greatly increase (see Fig. 12c).

The roots of the characteristic equation ($r_k = \pm\alpha_k \pm i\beta_k$) given by Eq. (23) are

$$\alpha_1 = 18.14 \qquad \alpha_2 = 26.09 \qquad \alpha_3 = 132.6$$
$$\beta_1 = 27.07 \qquad \beta_2 = 114.6 \qquad \beta_3 = 213.5 \tag{74}$$

This set of decay coefficients α_i confirm that vibrations are attenuated within a reasonable time; the settling times for particular modes are

$$t_1^{\text{eff}} = 0.1929\ \text{s} \qquad t_2^{\text{eff}} = 0.1342\ \text{s} \qquad t_3^{\text{eff}} = 0.02640\ \text{s} \tag{75}$$

The histograms of DOF d_x^{27} and d_y^{24} are shown in Figs. 12a and 12b, and actuation forces F_2 and F_5 are plotted Fig. 12c. Vibrations are attenuated more quickly than in cases 1–5 ($t_1^{\text{eff}} = 0.1929$ s), but the maximum forces required during the control period are about 2 GN, greater by seven orders of magnitude than in previous cases. The action of both actuators is indistinguishable in Fig. 12c, but they are indeed different. In fact, the difference between actuation forces, F_2–F_5 shown in Fig. 12d, is somewhat similar to the action of F_2 in case 2 (Fig. 9b). Despite the large forces ($\sim$2 GN) generated by each individual actuator, the magnitude of $(F_2–F_5)^{\max} \approx 92$ N is comparable to $F_2^{\max} \approx 121$ N.

The cause of uncharacteristically large forces in case 6 can be traced to the fact that the increase (decrease) in the distance between nodes 2 and 18 is nearly identical to the decrease (increase) in the distance between nodes 7 and 13 when the frame vibrates in the first and second modes (see Fig. 6b). Therefore, actuator F_5 essentially neutralizes the action of F_2 toward vibration attenuation instead of "helping" it. This, in turn, causes force F_2 to increase, followed by increasing F_5, and so on. Clearly, one of the actuators at these locations should be considered redundant.

In general, any case of redundant actuators, reflected in excessive actuation forces, will automatically produce a very large value of the effort parameter κ in Eq. (12b) (compare $\kappa = 74.46 \times 10^6$ for case 6 with $\kappa = 4.212$ for case 2).

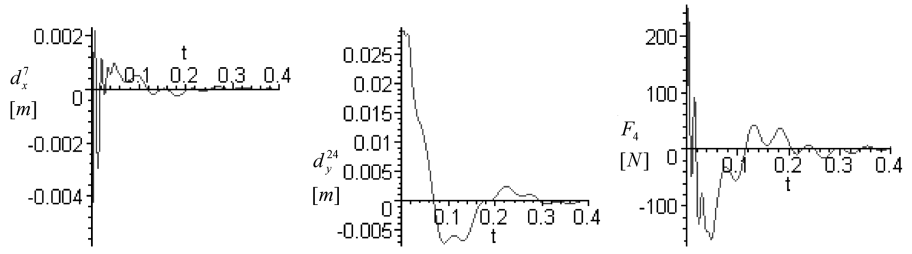

a) b) c)

Fig. 11 Case 5: a) response d_x^7, b) response d_y^{24}, and c) actuation force F_4.

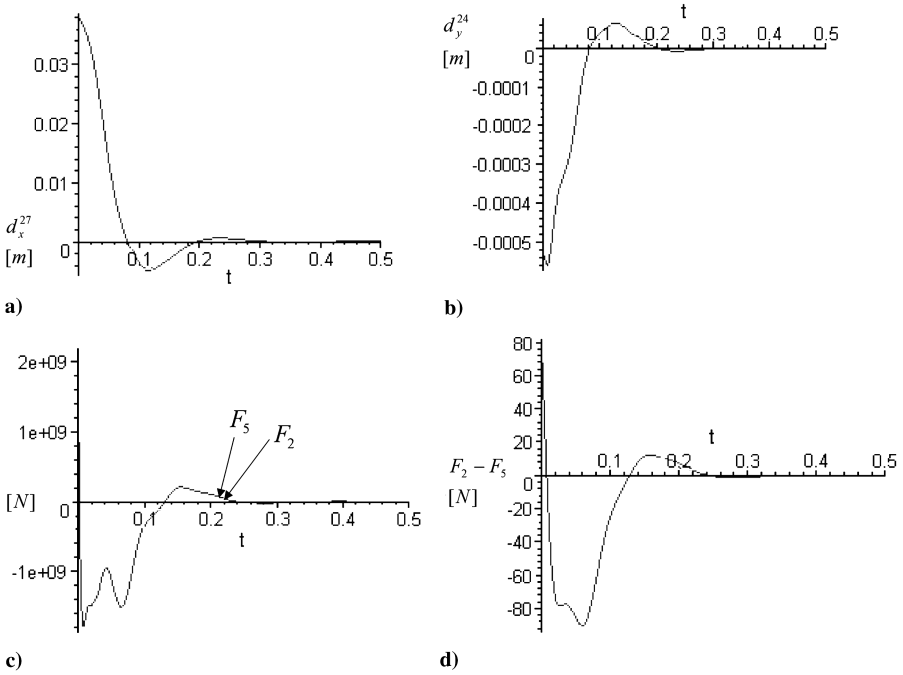

Fig. 12 Case 6: a) response d_x^{27}, b) response d_y^{24}, c) actuation force F_2, and d) actuation forces F_2–F_5.

G. Case 7 Actuators F_2 and F_3 to Control Three Modes

In case 7, a better (nonredundant) position of the second actuator to help actuator F_2 control the first three modes is considered. Actuators F_2 and F_3 from cases 2 and 3 ($n_a = 2$, $n_m = 3$, $n_r = 1$, and $n_t = 4$) are combined. With F_1 chosen as a dummy actuator, Eq. (8) becomes

$$\begin{bmatrix} F_a \\ F_d \end{bmatrix} = \begin{bmatrix} -1.871 & 0.1265 & 0.3834 \\ -2.097 & -0.6688 & -0.2668 \\ -1.341 & 0.6895 & -0.3246 \end{bmatrix} \begin{bmatrix} u_1 \\ u_2 \\ u_3 \end{bmatrix} = \begin{bmatrix} F_2 \\ F_3 \\ 0 \end{bmatrix} \tag{76}$$

The normalized constraint matrix (10) is

$$A = [\,1 \quad -0.5143 \quad 0.2421\,] \tag{77}$$

The elements of this matrix suggest adequate control over all three modes.

Actuation forces F_2 and F_3 in form (11) are

$$F_a = \bar{B}_a U_a = \begin{bmatrix} -3.455 & 0.9408 \\ -0.9950 & -1.235 \end{bmatrix} \begin{bmatrix} u_1 \\ u_2 \end{bmatrix} = \begin{bmatrix} F_2 \\ F_3 \end{bmatrix} \tag{78}$$

The controllability parameters from Eqs. (12a) and (12b) are

$$\lambda = 0.2421 \qquad \kappa = 5.203 \tag{79}$$

The rate parameter is similar to that in case 6, whereas the effort parameter κ is similar to that in cases 1–5, and so the expected attenuation times should be comparable with case 6 and the magnitude of actuation forces with cases 1–5.

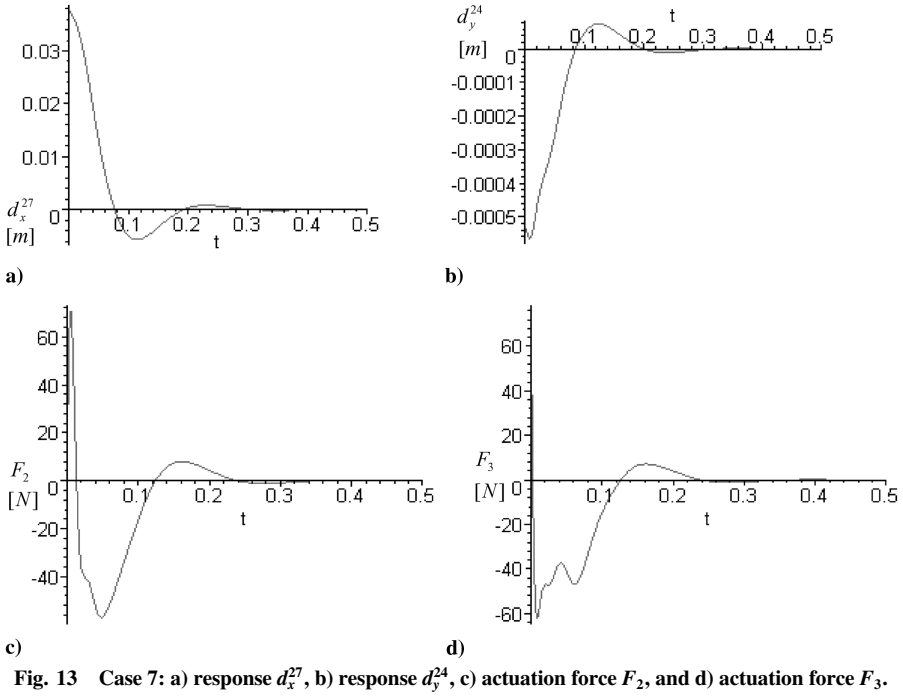

Fig. 13 Case 7: a) response d_x^{27}, b) response d_y^{24}, c) actuation force F_2, and d) actuation force F_3.

The roots of the characteristic equation ($r_k = \pm\alpha_k \pm i\beta_k$), given by Eq. (23), are

$$\alpha_1 = 16.77 \qquad \alpha_2 = 45.28 \qquad \alpha_3 = 114.9$$
$$\beta_1 = 27.28 \qquad \beta_2 = 115.9 \qquad \beta_3 = 212.7 \tag{80}$$

The effective settling times are

$$t_1^{\text{eff}} = 0.2087 \text{ s} \qquad t_2^{\text{eff}} = 0.07730 \text{ s} \qquad t_3^{\text{eff}} = 0.03046 \text{ s} \tag{81}$$

The disturbance is eliminated altogether in about 0.21 s, versus 0.19 s for case 6. Note that the combination of F_2 and F_3 can attenuate it faster than either actuator individually because 0.38 s was needed in case 2 and 0.33 s in case 3. The histograms of DOF d_x^{27} and d_y^{24} are shown in Figs. 13a and 13b, and actuation forces F_2 and F_3 are shown in Figs. 13c and 13d.

Unlike case 6, this configuration of actuators requires smaller forces than the actuation forces in either case 2 or 3. In fact, the maximum force in each actuator is $F_2^{\max} = 70$ N and $F_3^{\max} = 76$ N, their sum being only slightly greater than the maximum force for case 2 (121 N) or 3 (131 N).

Note that if the fourth mode was considered in cases 6 or 7, then similar to case 4 a very large value of parameter λ would be obtained to reflect slow attenuation of the fourth mode. However, matrix $\bar{B}_a$ would not be affected because there was no change in the actuator configuration.

VII. Conclusions

A procedure for analyzing and simulating active optimal vibration control of underactuated elastic structural systems is presented. Underactuation brings about certain constraints that the system must obey. These constraints, which are formulated using dummy actuators, are nonintegrable (nonholonomic) in terms of the modal variables (or the system's degrees of freedom) but algebraic (holonomic) in terms of the modal controls. The algebraic form of the modal controls' constraints can be used to formulate the normalized constraint matrix and the pseudotransfer matrix. These two matrices, which are determined in the early phase of the analysis, depend only on the placement of the actuators and therefore define the system's controllability. The attenuation rate and effort parameters, which are derived from the matrices herein, can be used to compare controllability of a system with different configurations of actuators.

The solution procedure combines the use of the FE and symbolic mathematics standard software to analyze and simulate the entire control process, including the actuation and the response histograms. As the examples demonstrate, a poor placement of actuators leading to an excessively long attenuation time of a particular mode is indicated by large numerical values of some coefficients of the constraint matrix or a large value of the rate parameter. In turn, large values of coefficients in the pseudotransfer matrix or a large value of the effort parameter signal redundant actuators, resulting in excessively large actuation forces. The aforementioned properties of the constraint and pseudotransfer matrices, or the controllability parameters, may be used for a preliminary assessment of the actuation setup, which can be done within the problem's structural analysis phase (and using only the FE software), without actually entering the control phase (i.e., without using the symbolic operations that require the mathematical software).

Appendix: Comments on Calculating Integration Constants

The relatively large number of integration constants required to determine the optimality equations' solutions in the form (28) is the consequence of additional differentiation operations [additional to the original operations already present in Eqs. (18) and (19)] that were performed to obtain the polynomial operator $\tilde{E}$. Therefore, Eq. (23) is of relatively high order and, when integrated, an identical number of additional integration constants are created. It should noted that Eqs. (23) and solutions (28) with all the numerical values of constants are automatically generated in MAPLE.

In Eqs. (28), there are $2(n_m)^2$ constants defining n_m modal variables η_j, and $2n_m n_c$ constants defining n_c Lagrange multipliers v_j. Because only $2n_m$ initial conditions (disturbances) can be assumed, the remaining $2n_m(n_t - 1)$ constants must be found by comparing terms in Eqs. (18) and (19). Note that factoring out $2n_m$ solving functions in Eqs. (19) provides $2n_m n_c$ linear equations with $2(n_m)^2$ constants c_{kj}^1, c_{kj}^2 related only to η_j, which when supplemented by $2n_m$ initial conditions provide $2n_m(n_c + 1)$ equations. When $n_c = n_m - 1$, or $n_a = 1$ (one actuator is to control several modes), the equations with the constants related to the modal variables can be solved independently of the constants related to the Lagrange multipliers. Because the latter constants are not used in the subsequent analysis, the numerical effort can be reduced by not calculating them at all (the left-out constants may be obtained from Eq. (18) if required). Otherwise, if multiple actuators are employed, all constants are interdependent and must be calculated simultaneously from Eqs. (18) and (19).

For the case of a single actuator ($n_a = 1$) in example I the integration constants defining the modal variables η_1 and η_2 can be found independently (without solving for the constants related to v_1). These eight constants are determined from the set of four homogeneous equations (37) and four initial conditions (31a) and (31b). The following numerical values were obtained for the integration constants:

$$\begin{aligned} c_{11}^1 &= 18.41 \times 10^{-3} & c_{12}^1 &= -6.208 \times 10^{-3} \\ c_{11}^2 &= 74.96 \times 10^{-3} & c_{12}^2 &= -.5594 \times 10^{-3} \\ c_{21}^1 &= 3.262 \times 10^{-3} & c_{22}^1 &= 6.624 \times 10^{-3} \\ c_{21}^2 &= -2.748 \times 10^{-3} & c_{22}^2 &= 21.18 \times 10^{-3} \end{aligned} \tag{A1}$$

The integration constants for the function v_1 are not shown, as they have no interpretive value in analyzing the suspension problem.

For the frame problem in example II, the solution of Eqs. (45a) and (45b) involves five functions ($\eta_1, \eta_2, \eta_3, v_1, v_2$), in the form (28), each containing six independent terms and six unknown integration constants, for a total of 30 ($2n_m n_t$) unknown constants. Substituting the solution functions into any four of the five equations in the set of Eqs. (45a) and (45b) and grouping similar terms renders sets of six algebraic equations for each differential equation, yielding 24 (four sets of six) algebraic equations all together. With the six boundary conditions (39), a total of 30 linear algebraic equations involving 30 unknown integration constants are obtained.

References

[1] Reyhanoglu, M., van der Schaft, A., McClamroch, N. H., and Kolmanovsky, I., "Dynamics and Control of a Class of Underactuated Mechanical Systems," *IEEE Transactions on Automatic Control*, Vol. 44, No. 9, 1999, pp. 1663–1671. doi:10.1109/9.788533

[2] Arai, H., Tanie, K., and Shiroma, N., "Nonholonomic Control of a Three-DOF Planar Underactuated Manipulator," *IEEE Transactions on Robotics and Automation*, Vol. 14, 1998, pp. 1–18. doi:10.1109/70.660834

[3] Bullo, F., and Lynch, K. M., "Kinematic Controllability for Decoupled Trajectory Planning in Underactuated Mechanical Systems," *IEEE Transactions on Robotics and Automation*, Vol. 17, No. 4, 2001, pp. 402–412. doi:10.1109/70.954753

[4] Hong, K.-S., "An Open-Loop Control for Underactuated Manipulators using Oscillatory Inputs: Steering Capability of an Unactuated Joint," *IEEE Transactions on Control Systems Technology*, Vol. 10, No. 3, 2002, pp. 469–480. doi:10.1109/87.998037

[5] Bathe, K.-J., "Modal Superposition," *Finite Elements Procedures*, Prentice–Hall, Englewood Cliffs, NJ, 1996, Chaps. 9.3.

[6] Fantoni, I., and Lozano, R., *Non-Linear Control for Underactuated Mechanical Systems*, Springer–Verlag, London, 2002.

[7] Craig, J. J., *Introduction to Robotic; Mechanics and Control*, Pearson Education, Upper Saddle River, NJ, 2005.

[8] Slotine, J.-J., and Weiping Li, *Applied Non-Linear Control*, Prentice–Hall, Upper Saddle River, NJ, 1991.
[9] Bayo, E., Papadopoulos, P., and Stubbe, J., "Inverse Dynamics and Kinematics of Multilink Elastic Robots: An Iterative Frequency Domain Approach," *International Journal of Robotics Research*, Vol. 8, 1989, pp. 49–62. doi:10.1177/027836498900800604
[10] De Jalon, J. G., and Bayo, E., *Kinematic and Dynamic Simulation of Multibody Systems—The Real-Time Challenge*, Springer–Verlag, Berlin/New York/Heidelberg, 1993, Chap. 12.
[11] Kwon, D.-S., and Book, W. J., "A Time-Domain Inverse Dynamic Tracking Control of a Single-Link Flexible Manipulator," *Journal of Dynamic Systems, Measurement, and Control*, Vol. 116, 1994, pp. 193–200. doi:10.1115/1.2899210
[12] Karihaloo, B. L., and Parbery, R. D., "Optimal Control of a Dynamical System Representing a Gantry Crane," *Journal of Optimization Theory and Applications*, Vol. 36, No. 3, 1982, pp. 409–417. doi:10.1007/BF00934354
[13] Spong, M. W., "The Swing Up Control problem for the Acrobot," *IEEE Control Systems Magazine*, Vol. 15, No. 1, 1995, pp. 49–55. doi:10.1109/37.341864
[14] Do, K. D., and Pan, J., "Global Tracking Control of Underactuated Ships with Nonzero Off-Diagonal Terms in Their System Matrices," *42nd IEEE Conference on Decision and Control*, Vol. 1, Institute of Electrical and Electronics Engineers Control Systems Society, 2003, pp. 1250–1255.
[15] Saimek, S., and Li, P. Y., "Motion Planning and Control of a Swimming Machine," *The International Journal of Robotics Research*, Vol. 23, No. 1, 2004, pp. 27–53. doi:10.1177/0278364904038366
[16] Hrovat, D., "Applications of Optimal Control to Advanced Automotive Suspension Design," *Journal of Dynamic Systems, Measurement, and Control*, Vol. 115, No. 2b, 1993, pp. 328–342. doi:10.1115/1.2899073
[17] Ju, F., Chao, Y. S., and Cui, F. S., "Dynamic Response of Tower Crane Induced by the Pendulum Motion of the Payload," *International Journal of Solids and Structures*, Vol. 43, 2006, pp. 376–389. doi:10.1016/j.ijsolstr.2005.03.078
[18] Saleh, A., and Adeli, H., "Algorithms for Solution of the Riccati Equation," *Control, Optimization, and Smart Structures*," Wiley, New York, 1999, Chap. 5.
[19] Calfield, R. A., and Meirovitch, L., "Integrated Structural Design and Vibration Suppression Using Independent Modal Space Control," *AIAA Journal*, Vol. 32, No. 10, 1994, pp. 2053–2060. doi:10.2514/3.12251
[20] Junkins, J. L., and Kim, Y. D., *Introduction to Dynamics and Control of Flexible Structures*, AIAA Education Series, AIAA, Washington, DC, 1993.
[21] Szyszkowski, W., and Grewal, I. S., "Beam Analogy for Optimal Control of Linear Dynamic Systems," *Computational Mechanics*, Vol. 25, 2000, pp. 489–501. doi:10.1007/s004660050496
[22] Szyszkowski, W., and Baweja, M., "Optimal Gains for Active Vibration Control by the Beam Analogy," *Computational Mechanics*, Vol. 34, 2004, pp. 15–26. doi:10.1007/s00466-004-0549-1
[23] Blajer, W., and Kolodziejczyk, K., "Control of Under-Actuated Mechanical Systems with Servo-Constraints ," *Nonlinear Dynamics*, Vol. 50, 2007, pp. 781–791. doi:10.1007/s11071-007-9231-4
[24] Fliess, M., Levine, J., Martin, P., and Rouchon, P., "Flatness and Defect of Nonlinear Systems: Introductory Theory and Examples," *International Journal of Control*, Vol. 61, 1995, pp. 1327–1361. doi:10.1080/00207179508921959

J. Cooper
Associate Editor